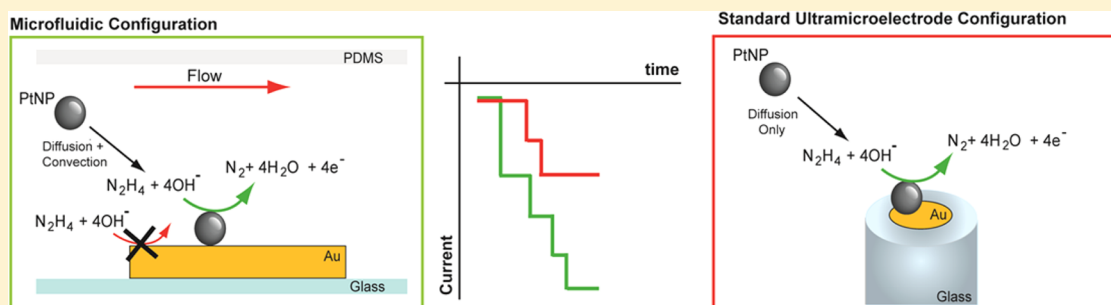


Single Nanoparticle Collisions at Microfluidic Microband Electrodes: The Effect of Electrode Material and Mass Transfer

Timothy M. Alligrant, Morgan J. Anderson, Radhika Dasari, Keith J. Stevenson,* and Richard M. Crooks*

Department of Chemistry and Center for Nano- and Molecular Science and Technology, The University of Texas at Austin, 105 East 24th Street, Stop A5300, Austin, Texas 78712-0165, United States

Supporting Information



ABSTRACT: We report on the effect of convection on electrochemically active collisions between individual Pt nanoparticles (PtNPs) and Hg and Au electrodes. Compared to standard electrochemical cells utilizing Hg and Au ultramicroelectrodes (UMEs) used in previous studies of electrocatalytic amplification, microelectrochemical devices offer two major advantages. First, the PtNP limit of detection (0.084 pM) is ~ 8 times lower than the lowest concentration measured using UMEs. Second, convection enhances the mass transfer of PtNPs to the electrode surface, which enhances the collision frequency from $\sim 0.02 \text{ pM}^{-1} \text{ s}^{-1}$ on UMEs to $\sim 0.07 \text{ pM}^{-1} \text{ s}^{-1}$ in microelectrochemical devices. We also show that the size of PtNPs can be measured in flowing systems using data from collision experiments and then validate this finding using multiphysics simulations.

INTRODUCTION

Electrocatalytic amplification (ECA) refers to the faradaic electrochemical response that results when a single, catalytic nanoparticle collides with a catalytically inactive electrode in the presence of an appropriate redox couple.^{1,2} This situation is illustrated in Scheme 1a. Here, a catalytic Pt nanoparticle (PtNP) collides with a noncatalytic Hg electrode. Once the PtNP collides with the electrode, hydrazine (N_2H_4) is electrocatalytically oxidized at the PtNP surface. This leads to the type of current transient shown to the right of the scheme.^{1,2} Experiments such as these are normally carried out in quiescent solutions using standard micro- or nanodisk electrodes (henceforth we refer to this configuration as a 'standard electrochemical cell').^{1,3,4} However, we recently showed that collision experiments can also be carried out in microelectrochemical devices under conditions of pressure driven flow (PDF).⁵ Microelectrochemical systems provide some key advantages, compared to standard electrochemical cells, for migrating fundamental studies of collision phenomena to sensor applications,^{5,6} and hence we have focused our attention on better understanding how the micron-scale channel, solution flow, and electrode type and configuration affect electrochemical responses. Here, we focus on the electrode material and solution flow.

ECA experiments are usually carried out by poisoning the working electrode (Au, Pt, PtO_x , carbon, or Hg) at a potential

where little faradaic current flows in the presence of an electroactive species (N_2H_4 , water, H_2O_2 , H^+ , O_2 , and BH_4^-).¹ Upon introduction of catalytic NPs (Au, Pt, or IrO_x), however, current transients are observed (*i-t* traces, Scheme 1). Each of these corresponds to a collision between a catalytic particle and the inert working electrode. As discussed later, the shape of the current transient depends on the details of the particular system under study. Important parameters include the size and material of the electrode and NPs,¹ the electrolyte⁷ and NP concentrations, the redox probe molecule undergoing the electrocatalytic reaction,¹ and the electrochemical detection method (chronoamperometry, potentiometry, or fast-scan voltammetry).^{1,2,8,9} The groups of Alpuche-Aviles,¹⁰ Andrees-cu,¹¹ Bard,^{1,3,8,12-14} Compton,¹⁵⁻¹⁸ Crooks,⁵ Koper,^{19,20} Macpherson,¹³ Stevenson,²¹⁻²³ Unwin,¹⁹ and Zhang^{3,9,14,24} have all contributed significantly to our understanding of these relationships, though many mysteries remain.

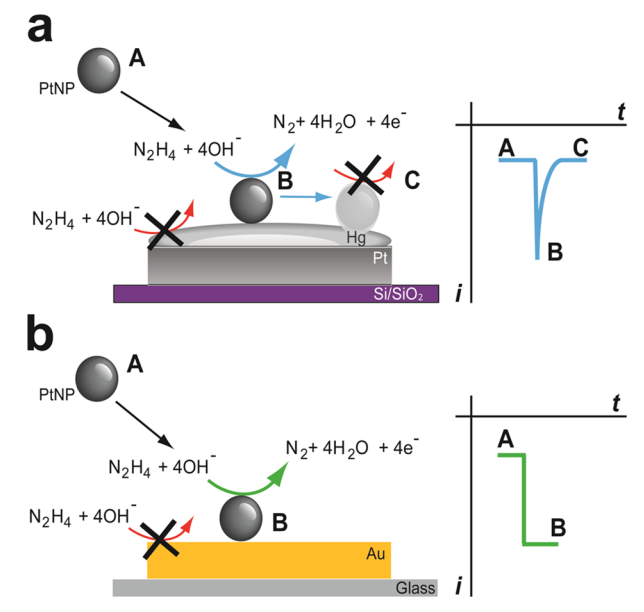
The work reported herein builds specifically on prior collision results from the Stevenson and Crooks groups. For example, the Stevenson group has shown that Hg electrodes lead to much higher signal-to-noise (S/N) levels than Au electrodes, primarily because of low faradaic background

Received: September 10, 2014

Revised: October 19, 2014

Published: October 31, 2014

Scheme 1



currents on Hg.^{21–23} Moreover, the shape of the collision-induced current transients at Hg electrodes is spike-shaped rather than stair-shaped (Scheme 1). We believe this is a consequence of rapid passivation of the colliding PtNP by Hg, as illustrated in Scheme 1a (point B to C).²¹ For sensing applications, both high S/N and spike-shaped current transients are desirable features.

The Crooks group previously utilized the ECA technique in microfluidic devices to observe the hybridization of single DNA strands in real-time.⁵ These microelectrochemical devices utilized a Au electrode modified with single-stranded DNA, poised at a potential where N_2H_4 was not readily oxidized. Upon flowing a N_2H_4 solution containing complementary DNA strands conjugated to PtNPs, current transients were observed. These corresponded to individual DNA hybridization events. However, one disadvantage of using ECA for DNA sensing applications involves the difficulty of distinguishing new hybridization events from collisions between previously hybridized PtNP-labeled DNA and the electrode surface. The rapid deactivation (poisoning) of the PtNPs by Hg should eliminate the possibility that each hybridization could lead to more than one faradaic current transient.

In the current ECA study, we compared collision dynamics using microelectrochemical cells outfitted with Hg and Au electrodes and using PtNP electrocatalysts and N_2H_4 as the sacrificial redox molecule. The results indicated that a PtNP limit of detection (LOD) as low as 0.084 pM can be achieved using a microelectrochemical cell. This compares to values in the range of 0.7 (Hg electrode)²¹ to 1.0 pM (Au electrode)² for detection of PtNPs using standard electrochemical cells. Moreover, collision frequencies of $\sim 0.069 \text{ pM}^{-1} \text{ s}^{-1}$ are attained in microelectrochemical devices, which are two to three times higher than the range achieved in standard electrochemical cells (0.02 and $0.024 \text{ pM}^{-1} \text{ s}^{-1}$ at Au and Hg electrodes, respectively).^{2,21} Finally, and in contrast to solid electrodes, Hg electrodes provide highly stable responses (flat baselines and uniform current transients) over long periods of time.²¹ All of these are desirable characteristics for future sensing applications that we envision.

EXPERIMENTAL SECTION

Chemicals and Materials. The following chemicals were purchased from Sigma-Aldrich (St. Louis, MO) and used as received: $N_2H_4 \cdot H_2O$ (64% N_2H_4 , 98%), H_2PtCl_6 (99.9%), $Hg(NO_3)_2$ (98.0%), and I_2 (99.8%). The following chemicals were purchased from Fisher Scientific (Fair Lawn, NJ) and used as received: $NaH_2PO_4 \cdot (H_2O)_2$ (100%), KNO_3 (100%), conc. HNO_3 , conc. HCl , and acetone (99.9%, HPLC grade). The following additional chemicals were used as received: $NaBH_4$ (98.0%, Acros Organics, Geel, Belgium), sodium citrate (99.0%, Alfa Aesar, Ward Hill, MA), ethanol (99.5%, anhydrous, Pharmco-AAPER, Brookfield, CT), and KI (100%, Mallinckrodt). Deionized water was obtained from a Millipore filtration system (Milli-Q gradient system, Millipore, Bedford, MA) and had a nominal resistivity of $18.2 \text{ M}\Omega \cdot \text{cm}$.

Synthesis of PtNPs. PtNPs were synthesized using a previously reported procedure.^{21,25} First, 7.76 mL of 0.2% (w/v) H_2PtCl_6 was added to 100 mL of boiling deionized water. Second, this solution was allowed to boil for ~ 1 min before adding 2.37 mL of a solution containing 1% (w/v) sodium citrate and 0.05% (w/v) citric acid. Third, the solution was allowed to boil for an additional ~ 30 s prior to addition of 1.18 mL of a freshly prepared solution containing 0.08% (w/v) $NaBH_4$, 1% (w/v) sodium citrate, and 0.05% (w/v) citric acid. The solution was then allowed to boil for an additional 10 min. Upon addition of the $NaBH_4$ solution, the color of the H_2PtCl_6 /citrate mixture became dark, indicating formation of PtNPs. Next, the product was cooled to 24–25 °C and then dialyzed for 24 h to remove excess salts.

Transmission electron microscopy (TEM, JEOL 2010F, JEOL Ltd., Tokyo, Japan) was used to determine the size (5.5 ± 2 nm) of the PtNPs (Figure S1a). The PtNP concentration was determined by dividing the concentration of the H_2PtCl_6 precursor by the number of Pt atoms²⁶ contained in a 5.5 nm particle.^{2,5,21} The PtNP concentration calculation is based on the assumption that all equivalents of H_2PtCl_6 are reduced to zerovalent PtNPs.

Device Fabrication. The microelectrochemical devices used for these experiments consist of two parts: a base, which supports the electrodes, and a polymeric fluidic system. For experiments involving Pt and Hg electrodes, the base consisted of a diced Si wafer having a 1 μm -thick oxide on its surface and photolithographically defined Pt microband electrodes (21 μm long). The Hg electrodes were prepared by electrodeposition of Hg onto the Pt electrodes. The Au electrodes (25 μm long) were photolithographically defined on a glass base without an adhesion layer. The procedures used to prepare the base and the electrodes have been reported previously and are discussed in detail in the Supporting Information.^{5,21–23}

The fluidic systems were cast into poly(dimethylsiloxane) (PDMS) using soft-lithography.²⁷ Complete fabrication details and photographs (Figure S2) are provided in the Supporting Information. The microchannels had dimensions of 6 mm (l) \times 25 (w) \times 18 μm (h) and reservoirs (either 1.2 or 4.0 mm in diameter, depending on flow setup, see the Supporting Information) were punched at the ends of the channels. Following fabrication, the PDMS fluidic system was exposed to an air plasma for 45 s and then immediately clamped to the base using a pair of polystyrene plates, to ensure uniform pressure, and a binder clip.

Electrochemical Experiments. Pressure-driven flow in the microelectrochemical devices was established using either gravity or a syringe pump. Details are provided in the Supporting Information.

Cyclic voltammetry (CV) and i - t curves obtained using microelectrochemical devices were measured using an electrochemical setup that was previously described.⁵ Briefly, a Chem-Clamp voltammeter-amperometer (Dagan Corp., Minneapolis, MN) served as the potentiostat, while the voltage signal was generated by a PAR 175 (Princeton Applied Research, Oak Ridge, TN) universal function generator. This setup was interfaced to a Dell Optiplex 380 computer through a PCI-6251 data acquisition board (National Instruments, Austin, TX) via a BNC-2090A analog breakout accessory (National Instruments, Austin, TX). Two-electrode cell connections from a preamplifier were housed in a Faraday cage constructed of copper

plate and wire mesh. The voltammetric data and i - t curves were measured using custom software written in LabView 2010 (National Instruments, Austin, TX). The sampling rate for measuring CVs and i - t curves was 50 Hz.

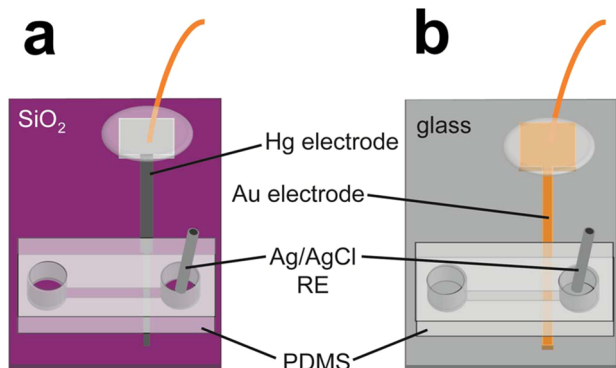
Electrochemical cleaning of the Si/SiO₂/Pt and glass/Au bases, Hg electrodeposition, and PtNP collision experiments in standard electrochemical cells were carried out using a CHI 650C potentiostat (CH Instruments, Austin, TX). All three-electrode electrochemical experiments (those performed using the CHI 650C potentiostat) utilized a Pt-counter electrode and a Ag/AgCl(1.0 M KCl) reference electrode (CH Instruments). All potentials reported herein were referenced to a "leakless" Ag/AgCl reference electrode (3.4 M KCl, model 66-EE009, Dionex, Bannockburn, IL) utilized for the microelectrochemical measurements. In addition, no electrochemical solutions, unless stated otherwise, were degassed prior to experiments.

Finite-Element Simulations. Finite-element simulations (FES) were performed using COMSOL Multiphysics v4.3 software and a Dell T7500 computer equipped with a Dual Six Core Intel Xeon processor (2.40 GHz) and 24 GB of RAM, running on a Windows 7 64-bit operating system. Full simulation details, including parameters, geometry, and discussion of results, are presented in the Supporting Information.

RESULTS AND DISCUSSION

Fluidics. The microelectrochemical cells used in the present work are illustrated in Scheme 2 and described in detail in the

Scheme 2



Experimental Section and the Supporting Information. Microelectrochemical devices having Hg electrodes were prepared by electrodepositing Hg over a Pt microband electrode patterned onto a Si/SiO₂ base (Scheme 2a). This results in a series of microdroplets, which is typical for electrodeposited Hg, rather than a flat, homogeneous coating (Figure S3).^{28,29} Accordingly, it was necessary to isolate a single Hg droplet within the microchannel during device assembly. The dimensions of the Hg working electrodes were defined by the width of the Pt microband (21 μ m) and the width of the channel (25 μ m), and they were hemispheroidal in shape with a height of 3.4 ± 2 μ m (Figure S4). Microelectrochemical devices incorporating Au electrodes were fabricated by photolithographically patterning a 25 μ m-wide Au microband onto a glass slide (Scheme 2b). Therefore, the Au electrodes had dimensions of 25 μ m \times 25 μ m and a height of ~ 0.1 μ m.

Once prepared, the bases were laminated with a PDMS monolith, embossed with a 6 mm (l) \times 25 (w) \times 18 μ m (h) microchannel and two 4.0 mm-diameter reservoirs, which served as the inlet and outlet. The microband electrodes were oriented perpendicular to the microchannel and were within ~ 500 μ m of the outlet reservoir, where the reference electrode resides, to minimize uncompensated solution resistance.³⁰

Unless indicated otherwise, PDF was established using differential heights of the solutions in the reservoirs. Gravity-driven flow resulted in volumetric flow rates of up to 10 nL min⁻¹.

PtNP Collisions at Hg Electrodes. Collision experiments using Hg electrodes were carried out using a microelectrochemical device like the one illustrated in Scheme 2a. The following procedure was used to obtain electrochemical data. First, flow of the electrolyte solution was established, and then a CV was obtained by scanning the Hg electrode potential from -0.20 to 0.20 at 0.020 V s⁻¹ in a solution containing 50.0 mM phosphate buffer (pH 7.5). In this case (dashed black line, Figure 1a), the current is very low and deviates from the

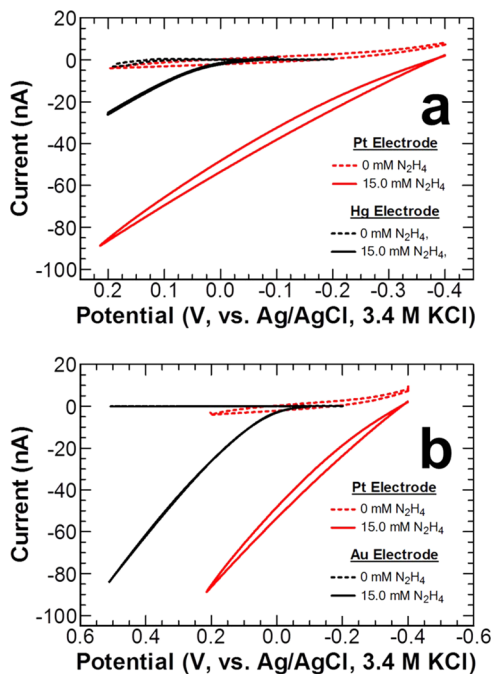


Figure 1. Representative CVs obtained using microelectrochemical devices in the absence (dashed traces) and presence (solid traces) of 15.0 mM N₂H₄ measured at (a) Hg and (b) Au electrodes. For comparison, CVs obtained using Pt electrodes are also shown (red traces). The scan rate was 0.020 V s⁻¹, the flow rate was 0.05 nL min⁻¹, and the electrolyte solution was 50.0 mM phosphate buffer (pH 7.5).

baseline only at the most extreme positive potentials due to Hg oxidation. Second, the solution was removed from the reservoirs and replaced with an identical solution, but this time containing 15.0 mM N₂H₄. The resulting CV (solid black line, Figure 1a) reveals a much larger current and an apparent onset potential of ~ 0 V due to N₂H₄ oxidation.^{21,23} In addition to the CVs measured at the Hg electrode, two CVs measured at a Pt electrode in the absence and presence of 15.0 mM N₂H₄ (dashed and solid red lines, respectively) are also presented in Figure 1a. Here, the onset for N₂H₄ oxidation occurs much earlier than on Hg (~ -0.4 V vs ~ 0 V), underscoring the catalytic properties of Pt relative to Hg.^{21,23}

The two black CVs in Figure 1a are important for selecting the correct potential for carrying out collision experiments. Specifically, the potential selected for recording i - t data should be sufficiently negative that little or no current arising from N₂H₄ oxidation is apparent on the Hg electrode, but it should be sufficiently positive that a measurable catalytic current is

observed when a PtNP collides with the Hg surface. Accordingly, and consistent with previous reports,^{21,23} we selected a potential of -0.050 V for the collision experiments carried out using the Hg electrodes.

Figures 2a–2c show representative sections of i - t recordings for PtNP collisions in the absence (black lines) and presence

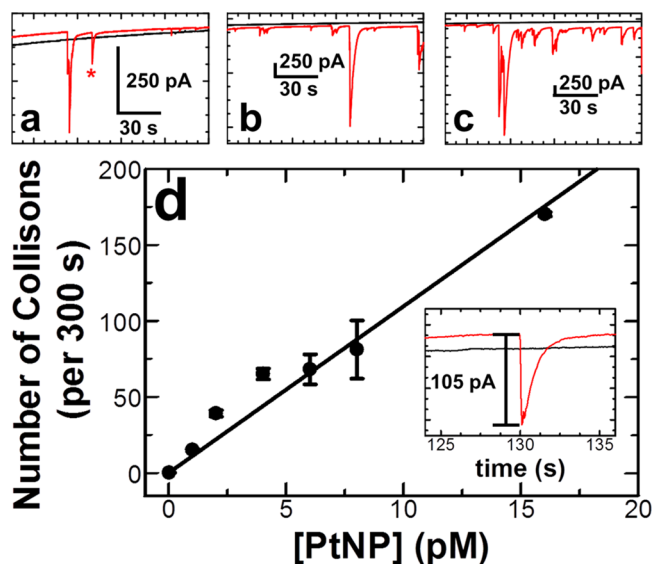


Figure 2. (a–c) Chronoamperometric (i - t) traces obtained using a microelectrochemical device outfitted with an Hg electrode in the absence (black trace) and presence (red traces) of 5.5 nm PtNPs at the following concentrations: (a) 1.0 pM, (b) 2.0 pM, and (c) 16 pM. The solution contained 15.0 mM N_2H_4 and 50.0 mM phosphate buffer (pH 7.5), the flow rate was 0.05 nL min^{-1} , and the Hg electrode potential was held at -0.050 V vs Ag/AgCl (3.4 M KCl). (d) Plot showing the correlation between the number of collisions (measured over 300 s) and concentration for 5.5 nm PtNPs. The error bars represent the standard deviation for three experiments per PtNP concentration. All data were obtained using a total of three independently prepared microelectrochemical devices. The inset in (d) shows an expanded view of the transient indicated by an asterisk in (a).

(red lines) of PtNPs (all collision experiments were carried out for a total of 600 s). In the absence of PtNPs, the i - t plots exhibit a near-constant current of ~ -0.62 nA, due to slow oxidation of N_2H_4 on the Hg electrode, but they are otherwise featureless.

The experiments represented by the red i - t traces were carried out after replacing the N_2H_4 /buffer solution in the channel with one that also contained PtNPs. All other conditions remained the same. The red line in Figure 2a, for example, is an i - t plot obtained using 1.0 pM PtNPs (5.5 nm diameter). In this case, clear spike-shaped current transients are observed due to collisions between the PtNPs and the Hg electrode. This shape is evident in the inset of Figure 2d, which shows an expanded view of the peak marked with an asterisk in Figure 2a. The baseline-subtracted peak currents in this experiment range from 24 to 1230 pA, which is larger than the range previously reported for similarly sized PtNPs in a standard electrochemical cell: ~ 45 – 70 pA for ~ 4.7 nm PtNPs.²¹ This difference may be due to partial aggregation of the PtNPs in our experiments.²⁰ The current transients persisted for ~ 2 to ~ 10 s, which is similar to previously reported results obtained in a standard electrochemical cell.²¹

The data in Figures 2b and 2c were obtained under the same conditions as Figure 2a but using PtNP concentrations of 2.0 and 16 pM, respectively. There is a clear, qualitative trend toward more collisions at higher concentrations of PtNPs. Note that control experiments carried out using the same concentration range of PtNPs but, in the absence of N_2H_4 , did not exhibit current transients (Figure S5a).

The number of collisions measured per 300 s of i - t data at six different PtNP concentrations (0 to 16 pM) are plotted in Figure 2d. These data were taken from experiments like those shown in Figures 2a–2c using a total of three independently prepared microelectrochemical devices for the entire PtNP concentration range. Only the first 300 s of the available 600 s of data were used to maintain consistency with previous studies.²¹ There is a nearly linear correlation ($R^2 = 0.94$) between the number of collisions and concentration. It is customary to normalize the frequency of the current transients to NP concentration (eq 1),^{1,2,21} and this operation leads to a frequency range of 0.034 to 0.065 $pM^{-1} s^{-1}$. This range is two to three times larger than that previously reported (0.024 $pM^{-1} s^{-1}$ for ~ 4.7 nm PtNPs)²¹ and measured by us (0.023 \pm 0.02 $pM^{-1} s^{-1}$ for ~ 5.5 nm PtNPs, Figure S6) using standard electrochemical cells. The higher collision frequencies observed in the microelectrochemical devices are due to enhanced (convective) mass transfer relative to diffusion.

$$\text{Frequency} = \frac{\text{Number of Collisions}}{([\text{PtNP}])(300\text{s})} \quad (1)$$

PtNP Collisions at Au Electrodes. In standard electrochemical cells, Hg electrodes give rise to higher S/N ratios and lower background currents for PtNP collisions, relative to Au electrodes, and the current transients are peak-shaped rather than stair-shaped.²¹ We wanted to learn if these comparisons were also valid under conditions of flow, so we fabricated and tested microelectrochemical devices having Au electrodes (Scheme 2b) and obtained electrochemical data similar to that described in the previous section for Hg electrodes.

Figure 1b displays CVs obtained using Au electrodes in the absence (dashed trace) and presence (solid trace) of N_2H_4 . The CV obtained in the absence of N_2H_4 is featureless over the entire potential range. In the presence of 15.0 mM N_2H_4 , however, an onset current arising from oxidation of N_2H_4 is apparent at ~ -0.05 V. For comparison, CVs obtained using Pt electrodes are also provided (these are the same CVs shown in Figure 1a). The catalytic properties of Pt relative to Au are apparent, and on the basis of these data we selected a potential of -0.050 V for collision experiments.

Figures 3a–3c are representative sections of i - t traces collected at -0.05 V in the absence (black trace, Figure 3a) and presence (red traces) of PtNPs at concentrations of 1.0, 2.0, and 16 pM, respectively. The featureless i - t trace in the absence of PtNPs exhibits a background current of ~ -2.2 nA, due to the slow oxidation of N_2H_4 on Au. Unlike the spike-shaped current transients observed on Hg electrodes, collisions at Au result in features that are more step-shaped (inset, Figure 3d), as has been found previously using standard electrochemical cells.² The current steps eventually decay toward the baseline value, but the deactivation time scale is much longer than was observed on the Hg electrodes. Additionally, the current steps, like those on Hg, are larger than those previously reported in standard electrochemical cells (40–160 pA, ~ 3.6 nm PtNPs)² displaying a range in amplitudes from 25 to 1100

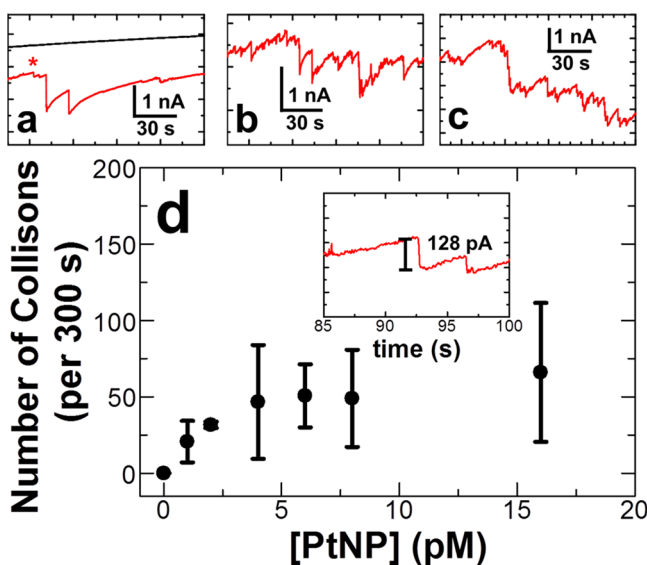


Figure 3. (a–c) Chronoamperometric (*i-t*) traces obtained using a microelectrochemical device outfitted with an Au electrode in the absence (black trace) and presence (red traces) of 5.5 nm PtNPs at the following concentrations: (a) 1.0 pM, (b) 2.0 pM, and (c) 16 pM. The solution contained 15.0 mM N_2H_4 and 50.0 mM phosphate buffer (pH 7.5), the flow rate was 0.05 nL min^{-1} , and the Au electrode potential was held at $-0.050 \text{ V vs Ag/AgCl (3.4 M KCl)}$. (d) Plot showing the correlation between the number of collisions (measured over 300 s) and concentration for 5.5 nm PtNPs. The error bars represent the standard deviation for three experiments per PtNP concentration. All data were obtained using a total of three independently prepared microelectrochemical devices. The inset in (d) shows an expanded view of the transient indicated by an asterisk in (a).

pA. Again, this could be a result of N_2H_4 -induced PtNP aggregation.²⁰

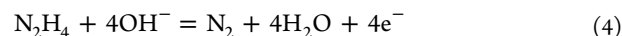
Figure 3d is a plot of the number of collisions measured during a 300 s time period for six different PtNP concentrations (0–16 pM). These data were extracted from *i-t* traces like those displayed in Figures 3a–3c. Unlike the Hg, there is no clear correlation between concentration and number of collisions in this case. This, and the large error bars, are probably a consequence of the fact that electrocatalytically active PtNPs accumulate on the Au surface and continue to catalyze N_2H_4 oxidation long after the original collision event is over. In contrast, recall that PtNPs are quickly deactivated when they strike the Hg electrode. The normalized collision frequencies (eq 1) over the six PtNP concentrations range from $0.014\text{--}0.069 \text{ pM}^{-1} \text{ s}^{-1}$. The maximum frequency obtained using microelectrochemical devices having Au electrodes is similar to that for Hg (0.069 vs $0.065 \text{ pM}^{-1} \text{ s}^{-1}$, respectively). However, the maximum frequency achieved using microelectrochemical devices having Au electrodes is two to three times larger than the maximum frequency reported ($0.02 \text{ pM}^{-1} \text{ s}^{-1}$ for $\sim 3.6 \text{ nm}$ PtNPs)² or measured by us ($0.019 \pm 0.006 \text{ pM}^{-1} \text{ s}^{-1}$, for $\sim 5.5 \text{ nm}$ PtNPs, Figure S6) in standard electrochemical cells outfitted with Au electrodes.

Collision-Based Sizing of PtNPs. Previously, the total charge (Hg electrodes)²¹ or current amplitude (Au electrodes)¹ from individual current transients, measured using standard electrochemical cells, has been used to estimate the size of PtNPs. Specifically, eq 2 expresses the charge (q) under each spike arising from the collision of a PtNP of radius r with a Hg

electrode.²¹ Likewise, eq 3 correlates the steady-state current (i_{ss}) amplitude to the radius of a PtNP colliding with an Au electrode.¹ The other variables in eqs 2 and 3 are as follows: n is the number of electrons transferred, which in this case is 4 (eq 4), F is the Faraday constant, D is the diffusion coefficient of N_2H_4 ($9.1 \times 10^{-6} \text{ cm}^2 \text{ s}^{-1}$),² C is the concentration of N_2H_4 (15.0 mM), and t represents time.^{1,21}

$$q = 4\pi(\ln 2)nFDCrt \quad (2)$$

$$i_{ss} = 4\pi(\ln 2)nFDCr \quad (3)$$



Though both eqs 2 and 3 neglect the influence of flow rate we considered their use in this system to be reasonable, because parabolic flow leads to low flow rates near the electrode surface.³¹ This approximation is given some credence by the close correspondence between the average size calculated using eqs 2 and 3 (5.1 ± 3 and $5.3 \pm 2 \text{ nm}$, respectively, Figure S7) and the size determined by TEM ($5.5 \pm 2 \text{ nm}$, Figure S1).

Multiphysics simulations were carried out to further validate the use of eqs 2 and 3 for describing PtNP collisions under flow conditions. We considered the case of a 5.5 nm sphere located on the channel floor and at various fixed heights above the electrode ($1.0\text{--}9.0 \mu\text{m}$) under flow (0.050 , 5.0 , and 50 nL min^{-1}) to evaluate the effects of convection. The simulation results show that the role of convection is negligible in relation to the collision amplitude. This is true when considering two key attributes: (1) the small size of the diffusion layer produced by the redox processes occurring at the PtNP surface and (2) the decreased linear flow velocity that occurs near the electrode surface (in the vicinity of the diffusion layer) due to edge effects. A complete discussion of the multiphysics simulations can be found in the Supporting Information.

Effect of Flow Rate on PtNP Collisions. Thus, far we have only discussed experimental results for a single flow rate: 0.05 nL min^{-1} . However, a clear advantage of microelectrochemical devices over standard electrochemical cells involves the ability to increase the rate of mass transfer of NPs to the working electrode via convection.

Figure 4 presents two plots of collision frequency as a function of flow rate at Hg (Figure 4a) and Au (Figure 4b) electrodes in the presence of 1.0 pM PtNPs. In both cases no collisions are observed under no-flow conditions (0 nL min^{-1}), because the NPs are delivered into one of the reservoirs rather than directly to the vicinity of the electrode (Scheme 2).

Over the range of flow rates examined (up to 50 nL min^{-1}), the collision data from microelectrochemical devices employing Hg electrodes can be described as having three frequency regimes. Initially, as the flow rate increases from 0.050 to 2.0 nL min^{-1} , the frequency of collisions increases from 0.0087 to 0.039 s^{-1} . The collision frequency then approaches a near-constant value of $\sim 0.03 \text{ s}^{-1}$ at flow rates between 2.0 and 10.0 nL min^{-1} . Finally, at 25.0 and 50.0 nL min^{-1} , the frequency decreases to 0.019 and 0.0042 s^{-1} , respectively. The situation for microelectrochemical devices having Au electrodes (Figure 4b) is somewhat different. At low flow rates (0.050 to 0.40 nL min^{-1}), the collision frequency remains constant at $\sim 0.040 \text{ s}^{-1}$. However, at higher flow rates the frequency decreases from 0.023 to 0 s^{-1} . Although we are unsure of the origin of the differences in the two plots shown in Figure 4, we speculate that there are three possibilities: (1) an unequal distribution of citrate-capped PtNPs in the channel under flow, (2) differences

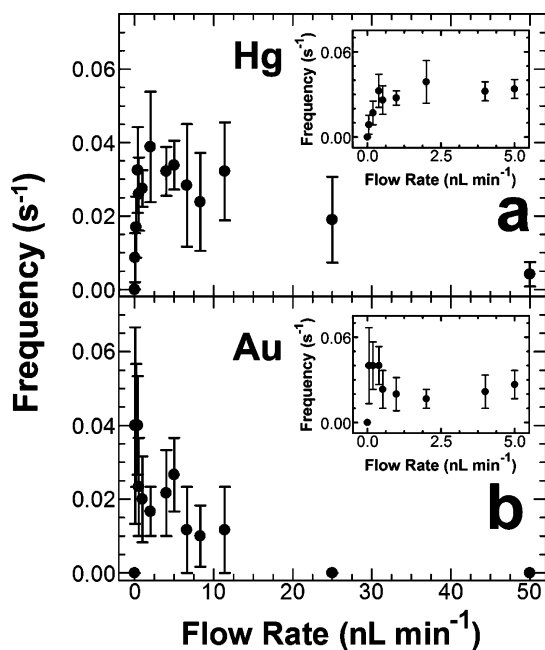


Figure 4. Plot of the collision frequency (measured over 600 s) as a function of flow rate measured at (a) Hg and (b) Au electrodes in microelectrochemical devices. The i - t curves used to construct this plot were measured using a solution containing 15.0 mM N_2H_4 , 50.0 mM phosphate buffer (pH 7.5), and 1.0 pM 5.5 nm PtNPs. The electrode potential was held at -0.05 V vs Ag/AgCl (3.4 M KCl). The insets represent expanded views of the low flow rate region. The error bars in both plots represent the standard deviation for three experiments per PtNP concentration. All data in (a) were obtained using a total of three independently prepared microelectrochemical devices having Hg electrodes. The data in (b) were obtained using 39 microelectrochemical devices having Au electrodes (three independently prepared devices per point).

in electrode geometry, and (3) physicochemical effects. These are discussed next.

Previous studies have found lower concentrations of NPs (diameter = 64–100 nm) near micro- and nanofluidic channel walls relative to their concentration in the center of the fluidic channel.^{32–35} These findings were attributed primarily to electrostatic repulsion between the negatively-charged particles and channel walls. Such electrostatic effects are influenced by the ionic strength of the solution used. In our studies the ionic strength is ~ 3 times higher than in an earlier report,³² but nevertheless electrostatic effects could play a role in determining the local concentration of PtNPs. Additionally, the Hg electrode (3.4 ± 2 μm in height) extends further into the fluidic channel than the Au electrode (0.1 μm in height). Because the Hg electrode extends away from the channel walls, it might be able to sample more PtNPs relative to Au electrodes. Additionally, differences in physicochemical parameters, such as the point-of-zero charge of the electrode, may have some influence on the results observed in Figure 4.

Because convection increases the rate of mass transfer of PtNPs in microelectrochemical devices, PtNP collisions should be observed at lower concentrations relative to electrodes in standard electrochemical cells. We tested this hypothesis by evaluating the LOD for collisions using the optimal flow rates (flow rates yielding the highest collision frequency). From Figure 4, the highest collision frequencies were measured at 2.0

(frequency = 0.039 s^{-1}) and 0.050 nL min^{-1} (frequency = 0.040 s^{-1}) on Hg and Au electrodes, respectively.

The LOD studies were carried out in a manner similar to that used to collect the data for Figures 2 and 3. The exceptions were the use of the aforementioned optimal flow rates, lower PtNP concentrations, and preparation of three independently prepared microelectrochemical devices having Au electrodes per PtNP concentration (The use of multiple devices in the case of Au electrodes is necessary because PtNPs adhere irreversibly to Au electrodes, and hence only a single collision experiment can be carried out on each device.).

Figure 5a displays a single i - t trace for 0.050 pM PtNPs flowing (2.0 nL min^{-1}) through a microelectrochemical device

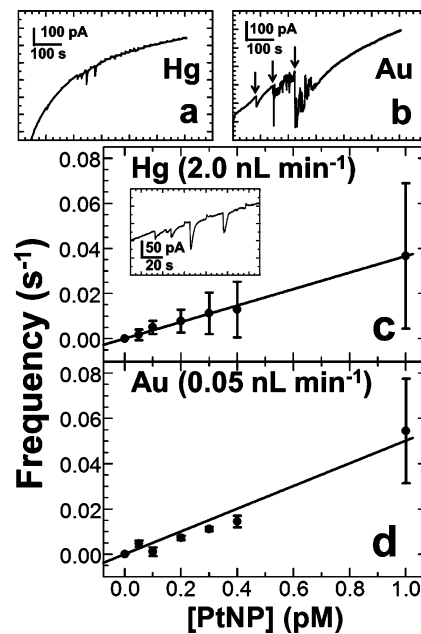


Figure 5. Chronoamperometric (i - t) traces obtained using microelectrochemical devices outfitted with (a) Hg and (b) Au electrodes. The solutions contained 15.0 mM N_2H_4 , 50.0 mM phosphate buffer (pH 7.5), and 0.050 pM PtNPs. The electrode potential was held at -0.05 V vs Ag/AgCl (3.4 M KCl). The flow rates were (a) 2.0 nL min^{-1} and (b) 0.05 nL min^{-1} . The arrows in (b) indicate the location of three collisions. (c–d) Plots of collision frequency (measured over 300 s) as a function of the concentration of 5.5 nm PtNPs. The error bars in (c) represent the standard deviation for three experiments per PtNP concentration. All data in (c) were obtained using a total of three independently prepared microelectrochemical devices. The error bars in (d) represent the standard deviation for three experiments per PtNP concentration. The data in (d) were obtained using a total of 18 independently prepared microelectrochemical devices (three devices per PtNP concentration). The inset in (c) shows an expanded view of four transients observed in (a).

having a Hg electrode. The part of this trace in which four collisions are observed is expanded in the inset (Figure 5c). Experiments like the one displayed in Figure 5a were replicated three times at six different PtNP concentrations. A plot of collision frequency as a function of PtNP concentration (Figure 5c) yields a linear correlation ($R^2 = 0.99$). Using these data, the LOD, calculated as 3 times the standard deviation divided by the slope, is 0.084 pM.³⁶ This value is more than eight times lower than the lowest PtNP concentration previously measured on Hg electrodes using standard electrochemical cells: 0.7 pM for ~ 4.7 nm PtNPs.²¹

Figure 5b displays an *i-t* trace recorded under similar conditions to that in Figure 5a, except the electrode was Au and the flow rate was 0.05 nL min⁻¹. In this case, just three collisions, indicated by arrows, are observed. On the basis of experiments like this, the LOD was determined to be 0.27 pM (Figure 5d). This LOD is nearly four times lower than the lowest PtNP concentration previously determined using Au electrodes within standard electrochemical cells: 1.0 pM for ~3.6 nm PtNP.²

SUMMARY AND CONCLUSIONS

In this report we have compared collision dynamics between PtNPs and Hg and Au electrodes under flowing conditions. The important results are as follows. First, the PtNP LOD was found to be as low as 0.084 pM in the microelectrochemical device, which is approximately eight times lower than the lowest PtNP concentration measured in a standard electrochemical cell. Second, convection enhances the mass transfer of PtNPs to the electrode surface, which increases the frequency of collisions from ~0.02 pM⁻¹ s⁻¹ in standard electrochemical cells to ~0.07 pM⁻¹ s⁻¹ in microelectrochemical devices. Third, we were able to determine the size of PtNPs as previously reported by both the Bard² and Stevenson²¹ groups. The role of convection is mixed: it enhances the rate of arrival of the PtNPs to the electrode surface, but it does not increase the current amplitude.

Our interest in ECA is currently directed toward using it as a method for chemical sensing (particularly for DNA), and the findings described here are important because they highlight some of the advantages and limitations of microelectrochemical cells for this purpose. The principle advantage of using microelectrochemical cells versus standard electrochemical cells involves the higher rate of mass transfer due to convection. However, we discovered that the distribution of PtNPs within the flow profile is irregular (Figure 4) and electrostatic repulsion may be responsible. If this is true, then it may be difficult to obtain similar LODs for DNA-modified PtNP conjugate collisions within a microelectrochemical device,⁵ given the negative charge of the DNA phosphodiester backbone (one negative charge per nucleotide). Currently, we are evaluating the use of both naked and single-stranded, thiolated DNA (ssDNA-SH) modified Hg electrodes in the presence of both ssDNA-SH-modified and naked PtNPs to determine the effect that DNA modification has on ECA experiments. There are a number of key questions that we hope to answer in forthcoming publications. For example, is it possible to decrease the influence of electrostatic repulsion by modifying the channel walls with a neutral surfactant or covalently linked monolayer (e.g., octadecyltrichlorosilane)³³ or by increasing the electrolyte concentration? Second, we have previously reported that very high collision frequencies (2.35×10^3 pM⁻¹ s⁻¹) can be obtained by enhancing mass transfer with magnetic fields.⁶ Those studies were carried out using microbeads, but we think it may be possible to gain this same advantage using nanoparticles having a magnetic core and a catalytic shell.^{37–39} Third, why are larger collision transients (~1 nA; Figure 2a–c and 3a–c) observed in microelectrochemical devices relative to standard electrochemical cells?

ASSOCIATED CONTENT

Supporting Information

Electron micrographs of PtNPs, additional device fabrication details, supplementary electrochemical data, electrochemical sizing of PtNPs, and details regarding finite element simulations (FESs). This material is available free of charge via the Internet at <http://pubs.acs.org>.

AUTHOR INFORMATION

Corresponding Authors

*Phone: 512-232-9160. E-mail: stevenson@cm.utexas.edu.

*Phone: 512-475-8674. E-mail: crooks@cm.utexas.edu.

Notes

The authors declare no competing financial interest.

ACKNOWLEDGMENTS

We gratefully acknowledge financial support from the U.S. Defense Threat Reduction Agency (Grant No. HDTRA1-11-1-0005). R.M.C. thanks the Robert A. Welch Foundation (Grant F-0032) for sustained research support. We would also like to thank Ms. Elizabeth G. Nettleton for preparing the Si/SiO₂/Pt substrates and Ms. Nellymar Membreno for the TEM images of the PtNPs. We are indebted to Prof. Allen J. Bard (UT Austin) and Prof. Bo Zhang (University of Washington) for helpful discussions. Additionally, we are grateful to Dr. Shouliang Zhang (TMI/CNM, UT Austin) for assistance with SEM measurements.

REFERENCES

- (1) Bard, A. J.; Zhou, H.; Kwon, S. J. Electrochemistry of Single Nanoparticles via Electrocatalytic Amplification. *Isr. J. Chem.* **2010**, *50*, 267–276.
- (2) Xiao, X.; Fan, F.-R. F.; Zhou, J.; Bard, A. J. Current Transients in Single Nanoparticle Collision Events. *J. Am. Chem. Soc.* **2008**, *130*, 16669–16677.
- (3) Park, J. H.; Thorgaard, S. N.; Zhang, B.; Bard, A. J. Single-Particle Detection by Area Amplification: Single-Wall Carbon Nanotube Attachment to a Nanoelectrode. *J. Am. Chem. Soc.* **2013**, *135*, 5258–5261.
- (4) Kim, J.; Kim, B.-K.; Cho, S. K.; Bard, A. J. Tunneling Ultramicroelectrode: Nanoelectrodes and Nanoparticle Collisions. *J. Am. Chem. Soc.* **2014**, *136*, 8173–8176.
- (5) Alligrant, T. M.; Nettleton, E. G.; Crooks, R. M. Electrochemical detection of individual DNA hybridization events. *Lab Chip* **2013**, *13*, 349–354.
- (6) Yoo, J. J.; Anderson, M. J.; Alligrant, T. M.; Crooks, R. M. Electrochemical Detection of Insulating Beads at Subattomolar Concentration via Magnetic Enrichment in a Microfluidic Device. *Anal. Chem.* **2014**, *86*, 4302–4307.
- (7) Park, J. H.; Boika, A.; Park, H. S.; Lee, H. C.; Bard, A. J. Single Collision Events of Conductive Nanoparticles Driven by Migration. *J. Phys. Chem. C* **2013**, *117*, 6651–6687.
- (8) Zhou, H.; Park, J. H.; Fan, F.-R. F.; Bard, A. J. Observation of Single Metal Nanoparticle Collisions by Open Circuit (Mixed) Potential Changes at an Ultramicroelectrode. *J. Am. Chem. Soc.* **2012**, *134*, 13212–13215.
- (9) Guo, Z.; Percival, S. J.; Zhang, B. Chemically Resolved Transient Collision Events of Single Electrocatalytic Nanoparticles. *J. Am. Chem. Soc.* **2014**, *136*, 8879–8882.
- (10) Fernando, A.; Parajuli, S.; Alpuche-Aviles, M. A. Observation of Individual Semiconducting Nanoparticle Collisions by Stochastic Photoelectrochemical Currents. *J. Am. Chem. Soc.* **2013**, *135*, 10894–10897.
- (11) Sardesai, N. P.; Andreescu, D.; Andreescu, S. Electroanalytical Evaluation of Antioxidant Activity of Cerium Oxide Nanoparticles by

Nanoparticle Collisions at Microelectrodes. *J. Am. Chem. Soc.* **2013**, *135*, 16770–16773.

(12) Kwon, S. J.; Bard, A. J. Analysis of Diffusion-Controlled Stochastic Events of Iridium Oxide Single-Nanoparticle Collisions by Scanning Electrochemical Microscopy. *J. Am. Chem. Soc.* **2012**, *134*, 7102–7108.

(13) Wakerley, D.; Güell, A. G.; Hutton, L. A.; Miller, T. S.; Bard, A. J.; Macpherson, J. V. Boron doped diamond ultramicroelectrodes: a generic platform for sensing single nanoparticle electrocatalytic collisions. *Chem. Commun.* **2013**, *49*, 5657–5659.

(14) Park, J. H.; Zhou, H.; Percival, S. J.; Zhang, B.; Fan, F.-R. F.; Bard, A. J. Open Circuit (Mixed) Potential Changes Upon Contact Between Different Intert Electrodes-Size and Kinetic Effects. *Anal. Chem.* **2013**, *85*, 964–970.

(15) Rees, N. V.; Zhou, Y.-G.; Compton, R. G. Making contact: charge transfer during particle-electrode collisions. *RSC Adv.* **2012**, *2*, 379–384.

(16) Zhou, Y.-G.; Rees, N. V.; Compton, R. G. The Electrochemical Detection and Characterization of Silver Nanoparticles in Aqueous Solution. *Angew. Chem., Int. Ed.* **2011**, *50*, 4219–4221.

(17) Zhou, Y.-G.; Rees, N. V.; Compton, R. G. The electrochemical detection of tagged nanoparticles via particle-electrode collisions: nanoelectroanalysis beyond immobilisation. *Chem. Commun.* **2012**, *48*, 2510–2512.

(18) Ly, L. S. Y.; Batchelor-McAuley, C.; Tschulik, K.; Kätelhön, E.; Compton, R. G. A Critical Evaluation of the Interpretation of Electrocatalytic Nanoimpacts. *J. Phys. Chem. C* **2014**, *118*, 17756–17763.

(19) Kleijn, S. E. F.; Lai, S. C. S.; Miller, T. S.; Yanson, A. I.; Koper, M. T. M.; Unwin, P. R. Landing and Catalytic Characterization of Individual Nanoparticles on Electrode Surfaces. *J. Am. Chem. Soc.* **2012**, *134*, 18558–18561.

(20) Kleijn, S. E. F.; Serrano Bou, B.; Yanson, A. I.; Koper, M. T. M. Influence of Hydrazine-Induced Aggregation on the Electrochemical Detection of Platinum Nanoparticles. *Langmuir* **2013**, *29*, 2054–2064.

(21) Dasari, R.; Robinson, D. A.; Stevenson, K. J. Ultrasensitive Electroanalytical Tool for Detecting, Sizing, and Evaluating the Catalytic Activity of Platinum Nanoparticles. *J. Am. Chem. Soc.* **2013**, *135*, 570–573.

(22) Dasari, R.; Walther, B.; Robinson, D. A.; Stevenson, K. J. Influence of the Redox Indicator Reaction on Single Nanoparticle Collisions at Mercury and Bismuth Modified Pt Ultramicroelectrodes. *Langmuir* **2013**, *29*, 15100–15106.

(23) Dasari, R.; Tai, K.; Robinson, D. A.; Stevenson, K. J. Electrochemical Monitoring of Single Nanoparticle Collisions at Mercury-Modified Platinum Ultramicroelectrodes. *ACS Nano* **2014**, *8*, 4539–4546.

(24) Kwon, S. J.; Zhou, H.; Fan, F.-R. F.; Vorobyev, V.; Zhang, B.; Bard, A. J. Stochastic electrochemistry with electrocatalytic nanoparticles at inert ultramicroelectrodes—theory and experiments. *Phys. Chem. Chem. Phys.* **2011**, *13*, 5394–5402.

(25) Bigall, N. C.; Härtling, T.; Klose, M.; Simon, P.; Eng, L. M.; Eychemüller, A. Monodisperse Platinum Nanospheres with Adjustable Diameters from 10 to 100 nm: Synthesis and Distinct Optical Properties. *Nano Lett.* **2008**, *8*, 4588–4592.

(26) Jentys, A. Estimation of the mean size and shape of small metal particles by EXAFS. *Phys. Chem. Chem. Phys.* **1999**, *1*, 4059–4063.

(27) Xia, Y.; Whitesides, G. M. Soft Lithography. *Angew. Chem., Int. Ed.* **1998**, *37*, 550–575.

(28) Powell, M.; Ball, J. C.; Tsai, Y.-C.; Suarez, M. F.; Compton, R. G. Square Wave Anodic Stripping Voltammetry at Mercury-Plated Electrodes. Simulation of Surface Morphology Effects on Electrochemically Reversible, Irreversible, and Quasi-reversible Processes: Comparison of Thin Films and Microdroplets. *J. Phys. Chem. B* **2000**, *104*, 8268–8278.

(29) Wu, H. P. Nature and Stability of Mercury Thin Films on Glassy Carbon Electrodes under Fast-Scan Anodic Stripping Voltammetry. *Anal. Chem.* **1994**, *66*, 3151–3157.

(30) Bard, A. J.; Faulkner, L. R. *Electrochemical Methods: Fundamentals and Applications*; Wiley: New York, 2000.

(31) Cooper, J. A.; Compton, R. G. Channel Electrodes - A Review. *Electroanalysis* **1998**, *10*, 141–155.

(32) Li, H. F.; Yoda, M. Multilayer nano-particle image velocimetry (MnPIV) in microscale Poiseuille flows. *Meas. Sci. Technol.* **2008**, *19*, 075402–075410.

(33) Yoda, M.; Li, H. An experimental study of slip considering the effects of non-uniform colloidal tracer distributions. *J. Fluid Mech.* **2010**, *662*, 269–287.

(34) Kazoe, Y.; Iseki, K.; Mawatari, K.; Kitamori, T. Evanescent Wave-Based Particle Tracking Velocimetry for Nanochannel Flows. *Anal. Chem.* **2013**, *85*, 10780–10786.

(35) Kanda, K.; Ogata, S.; Jingu, K.; Yang, M. Measurement of Particle Distribution in Microchannel Flow Using a 3D-TIRFM Technique. *J. Vis.* **2007**, *10*, 207–215.

(36) Long, G. L.; Winefordner, J. D. Limit of Detection: A Closer Look at the IUPAC Definition. *Anal. Chem.* **1983**, *55*, 712A–724A.

(37) Robinson, D. A.; Stevenson, K. J. Uniform epitaxial growth of Pt on Fe₃O₄ Nanoparticles; synergetic enhancement to Pt activity for the oxygen reduction reaction. *J. Mater. Chem. A* **2013**, *1*, 13443–13453.

(38) Melo, A. F. A. A.; Carvalho, V. A. N.; Pagnoncelli, K. C.; Crespilho, F. N. Single microparticle applied in magnetic-switchable electrochemistry. *Electrochem. Commun.* **2013**, *30*, 79–82.

(39) Santos, G. P.; Melo, A. F. A. A.; Crespilho, F. N. Magnetically controlled single-nanoparticle detection via particle-electrode collisions. *Phys. Chem. Chem. Phys.* **2014**, *16*, 8012–8018.